

FANeRV: Frequency Separation and Augmentation based Neural Representation for Video

Li Yu, Zhihui Li, Jimin Xiao, and Moncef Gabbouj, *Fellow, IEEE*

Abstract—Neural representations for video (NeRV) have gained considerable attention for their strong performance across various video tasks. However, existing NeRV methods often struggle to capture fine spatial details, resulting in vague reconstructions. In this paper, we present a Frequency Separation and Augmentation based Neural Representation for video (FANeRV), which addresses these limitations with its core Wavelet Frequency Upgrade Block. This block explicitly separates input frames into high and low-frequency components using discrete wavelet transform, followed by targeted enhancement using specialized modules. A specially designed gated network effectively fuses these frequency components for optimal reconstruction. Additionally, convolutional residual enhancement blocks are integrated into the later stages of the network to balance parameter distribution and improve the restoration of high-frequency details. Experimental results demonstrate that FANeRV significantly improves reconstruction performance and excels in multiple tasks, including video compression, inpainting, and interpolation, outperforming existing NeRV methods.

Index Terms—Video compression, Implicit neural representation, Neural representation for video, Wavelet transform

I. INTRODUCTION

Implicit Neural Representations (INRs) have attracted significant attention for their remarkable ability to accurately represent diverse signals [1]–[3]. NeRV [4] demonstrates the potential of INR in video representation. NeRV introduces a frame-based implicit representation that utilizes convolutional layers to map frame indices directly to video frames. It addresses issues such as slow training and poor reconstruction quality in pixel-based implicit representations [5], while demonstrating its potential across a variety of tasks, including video compression, interpolation, and inpainting. Building on this paradigm, subsequent works [6]–[8] have focused on designing more efficient network structures and embedding methods to further improve video reconstruction quality.

Despite these advancements, neural networks are constrained by spectral bias [9], which limits their ability to effectively capture fine spatial details, resulting in blurry video frame reconstruction. To address this issue, some studies [10], [11] encode high-frequency embeddings to improve detail recovery. However, these additional feature embeddings increase both network parameters and computational overhead. Other approaches [12], [13] adopt residual concatenation strategies, integrating low-resolution features from earlier stages to accelerate high-frequency learning and enhance reconstruction quality. However, improper upsampling alignment in these methods can cause frequency aliasing, impeding further performance improvements. Additionally, existing methods do not explicitly separate and learn high and low-frequency

components. Instead, they employ a uniform approach to all frequency components, making it challenging to emphasize high-frequency details while retaining the richness of low-frequency features.

To address these challenges, we propose the Frequency Separation and Augmentation based Neural Representation for video (FANeRV), designed to enhance the recovery of high-frequency details in frame reconstruction. Our method employs discrete wavelet transforms to explicitly decompose input features into high and low-frequency components, followed by applying targeted enhancement modules for each. Additionally, low-resolution features are fused with low-frequency subband to reinforce gradient flow and direct the network’s focus toward high-frequency details, enabling the precise capture of subtle spatial variations. To this end, we propose a Wavelet Frequency Upgrade Block (WFUB), which comprises two key components: the Frequency Separation Feature Boosting (FSFB) module and the Time-Modulated Gated Feed-Forward Network (TGFN). The FSFB module contains a multi-resolution deep feature modulation branch for capturing non-local dependencies, and a small-kernel residual branch to model local details features. The synergy of these sub-branches enables the FSFB module to effectively extract and integrate features across high and low-frequency components. Following this, the TGFN component refines the fused features across spatial and channel dimensions, focusing the network’s attention on regions with rich information. Furthermore, we integrate convolutional residual enhancement blocks in the later stages of the network to optimize parameter distribution and enhance precision in reconstructing high-frequency details.

Our primary contributions are as follows:

- We introduce FANeRV, which employs wavelet transforms to decompose high and low-frequency components, and designs enhancement fusion strategies tailored to their characteristics. By integrating lower-resolution features, FANeRV efficiently leverages multi-scale and multi-frequency information to improve reconstruction quality and detail accuracy.
- We develop the FSFB module, which consists of a low-frequency branch for capturing non-local dependencies and a high-frequency branch for modeling local textures. To improve feature integration, we incorporate the TGFN to effectively refine the fused features. Additionally, convolutional residual enhancement blocks are integrated into the network’s later stages to optimize parameter distribution and improve its capacity for reconstructing high-frequency details.

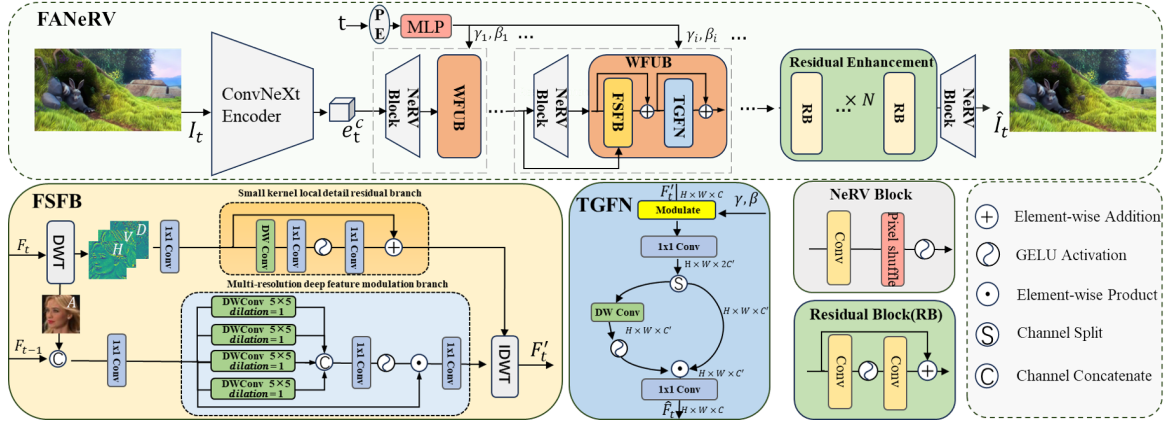


Fig. 1. Architecture of the proposed FANeRV. FANeRV integrates the Wavelet Frequency Upgrade Block (WFUB) and the convolutional residual enhancement block to enhance detail reconstruction. The WFUB comprises a Separation Feature Boosting (FSFB) module and a Time-Modulated Gated Feed-Forward Network (TGFN).

- We conduct comprehensive experiments, demonstrating that FANeRV achieves significant performance improvements across multiple tasks, including video regression, video compression, image inpainting, and interpolation, outperforming a wide range of baseline models.

II. PROPOSED METHOD

We begin by presenting an overview of our method pipeline in Section II-A. Next, we delve into the details of the proposed representation network in Sections II-B and II-C. Finally, we outline the loss function in Section II-D.

A. Overview.

Fig. 1 illustrates the architecture of the proposed Frequency Separation and Augmentation based Neural Representation for video (FANeRV). FANeRV employs a hybrid approach [7] for video representation, comprising content-related feature embeddings and decoder parameters. Specifically, given a video frame sequence $V = \{I_0, I_1, \dots, I_{T-1}\}$, where $I_t \in \mathbb{R}^{H \times W \times C}$ represents the frame at timestamp t with height H , width W , and channels C . The input frames I_t are initially downsampled to generate compact, content-related feature embeddings e_t^c via a ConvNeXt encoder E , which consists of stacked ConvNeXt blocks [14]. These embeddings e_t^c are then processed by the decoder, which is composed of a series of NeRV blocks [7] and Wavelet Frequency Upgrade Blocks (WFUB), to perform feature upsampling and refinement. In parallel, a temporal modulation network injects time information into the intermediate features at each stage, ensuring effective alignment during decoding. Finally, the refined features are passed through stacked convolutional residual enhancement blocks, yielding the final high-quality reconstruction.

B. Wavelet Frequency Upgrade Block

In image restoration and reconstruction tasks, preserving and enhancing high-frequency features is critical for achieving

high visual fidelity. Research has demonstrated that independently amplifying high and low-frequency features is an effective strategy [15]–[17]. Inspired by this, we proposed the WFUB to explicitly separate and strengthen high and low-frequency components. It consists of the Frequency Separation Feature Boosting (FSFB) module and Time-Modulated Gated Feed-Forward Network (TGFN). Specifically, given an input feature $F_t \in \mathbb{R}^{H \times W \times C}$, where $H \times W$ denotes the spatial dimensions and C represents the number of channels, we employ the Haar wavelet transform [18] to decompose each F_t into high and low-frequency components, resulting in four subbands:

$$\{A_{LL}^t, H_{LR}^t, V_{RL}^t, D_{RR}^t\} = \text{DWT}(F_t)$$

Here, A_{LL}^t represents the low-frequency subband containing global structural information, while H_{LR}^t , V_{RL}^t , and D_{RR}^t are high-frequency subbands capturing horizontal, vertical, and diagonal texture details. Each subband has dimensions $\mathbb{R}^{H/2 \times W/2 \times C}$. Additionally, to utilize low-resolution features F_{t-1}^{i-1} from the previous stage, which primarily contain low-frequency information, we concatenate A_{LL}^t with F_{t-1}^{i-1} to form enhanced low-frequency components.

After obtaining the explicitly extracted high-frequency components and enhanced low-frequency components, we apply a 1×1 convolution to transform them into initial high and low-frequency features. Next, we apply the proposed multi-resolution deep feature modulation branch \mathcal{LB} to capture global dependencies across scales and the small-kernel residual branch \mathcal{HB} to enhance local texture details. These branches work together to model both local and global features, enabling precise reconstruction. This process is defined as:

$$\{\hat{F}_l^t, \hat{F}_h^t\} = \mathcal{LB}(\text{Conv}1 \times 1(\text{Concat}(A_{LL}^t, F_{t-1}^{i-1}))), \\ \mathcal{HB}(\text{Conv}1 \times 1((H_{LR}^t, V_{RL}^t, D_{RR}^t))) \quad (1)$$

where $\hat{F}_l^t \in \mathbb{R}^{H/2 \times W/2 \times C}$ and $\hat{F}_h^t \in \mathbb{R}^{H/2 \times W/2 \times 3C}$ are the refined low-frequency and high-frequency features, respectively. Next, we employ the inverse discrete wavelet transform

(IDWT) to merge \hat{F}_l^t and \hat{F}_h^t , producing an initial fused feature F_t' . To further integrate these features and incorporate temporal embedding at each stage, we utilize TGFN to dynamically select the most representative features, refining the fused and time-modulated output. The process is defined as:

$$F_t' = \text{IDWT}(F_l^t, F_h^t) + F_t, \quad (2)$$

$$\gamma_i, \beta_i = \text{MLP}(\text{PE}(t)), \quad (3)$$

$$\hat{F}_t = \text{TGFN}(F_t' | \gamma_i, \beta_i) + F_t'. \quad (4)$$

where PE is the positional encoding function [1], MLP is a small multi-layer perceptron, and γ_i and β_i are affine parameters derived from temporal embeddings t . Finally, \hat{F}_t represents the final output of the WFUB.

1) *Multi-Resolution Deep Feature Modulation Branch*: Low-frequency features are essential for capturing structural and global characteristics in images. Exploring non-local feature interactions is crucial for their effective restoration. While existing methods use self-attention mechanisms or large kernel convolutions to explore non-local information and achieve strong reconstruction performance, they are often computationally expensive and are parameter-intensive. To address these challenges, we propose a lightweight approach for learning long-range dependencies from multi-scale feature representations. As shown in Fig. 1, we employ parallel depthwise separable dilated convolutions with varying kernel sizes and dilation rates to construct multi-scale feature maps f_l^j that capture low-frequency features at different scales. Specifically, given an input feature $F_l^t \in \mathbb{R}^{H \times W \times C}$, where H and W are the spatial dimensions and C is the number of channels, this procedure can be expressed as:

$$f_l^j = \text{DWConv}_{k_j \times k_j}(F_l^t, d_j), \quad 0 \leq j \leq 3 \quad (5)$$

where $\text{DWConv}_{k_j \times k_j}(\cdot)$ denotes a depthwise separable convolution with kernel size k_j and dilation rate d_j , specifically set as $k_j = [5, 7, 9, 11]$ and $d_j = [1, 2, 3, 4]$. To aggregate features from multi-scale low-frequency representations, we incorporate a gating mechanism to adaptively select the most representative features. we concatenat these features and then apply a 1×1 convolutional layer to produce a refined global feature representation that captures multi-order contexts. The GELU activation function [19] is then applied for nonlinear normalization, generating an attention map. This attention map is element-wise multiplied with the input features, enabling adaptive feature modulation that emphasizes critical features while dynamically adjusting the contribution of each scale. Finally, another 1×1 convolutional layer models the inter-channel relationships, generating the final output \hat{F}_l^t :

$$S = \sigma(\text{Conv}_{1 \times 1}(\text{Concat}([f_l^0, f_l^1, f_l^2, f_l^3]))) \quad (6)$$

$$\hat{F}_l^t = \text{Conv}_{1 \times 1}(S \odot F_l^t) \quad (7)$$

where $\sigma(\cdot)$ represents the GELU activation function, and \odot denotes element-wise product. This approach maintains computational efficiency while improving the network's capability to handle global structural information in images.

2) *Small Kernel Local Detail Residual Branch*: High-frequency features represent essential local details in images, crucial for high-quality reconstruction. To restore finer details, it is necessary to use smaller receptive fields that focus more precisely on local image information. Thus, we propose the Small-Kernel Local Detail Residual Block. Small convolution kernels enhance the focus on local details, while residual connections effectively capture high-frequency information. Specifically, the 3×3 depthwise convolution encodes local information f_h from the input F_h^t while expanding the channel count for enhanced channel mixing. Then, we use two 1×1 convolutions to further explore channel information and generate the enhanced local feature \hat{F}_h^t , which is achieved by:

$$f_h = \text{Conv}_{1 \times 1}(\text{DWConv}_{3 \times 3}(F_h^t)) \quad (8)$$

$$\hat{F}_h^t = \text{Conv}_{1 \times 1}(\sigma(f_h)) + F_h^t \quad (9)$$

where $\sigma(\cdot)$ denotes the GELU activation function.

3) *Time-Modulated Gated Feed-Forward Network*: To effectively fuse low-frequency and high-frequency features, we introduce a gating network that dynamically selects and integrates features, thereby reducing redundant processing. Moreover, the integration of temporal context at each stage enhances regression performance, accelerates model convergence, and improves the overall quality of the results [6]. To achieve this, temporal information is embedded into the intermediate features prior to the application of convolutional gating. Specifically, the input features F_i' are first linearly transformed using modulation parameters γ_i and β_i derived from temporal embeddings:

$$f_t^{\text{modulate}} = F_t' \odot (1 + \gamma_i) + \beta_i \quad (10)$$

A 1×1 convolution with GELU activation is then applied for cross-channel interaction in the expanded hidden space. The output is split into two components, a and x . Component a undergoes a 3×3 depthwise convolution to capture local spatial patterns, followed by a GELU non-linearity to estimate the attention map. This estimated attention is then used to adaptively modulate x through an element-wise product. Finally, a 1×1 convolution mixes features and reduces channel dimensions to match the input. The process is described by:

$$f_a, f_x = \text{Split}(\text{Conv}_{1 \times 1}(f_t^{\text{modulate}})) \quad (11)$$

$$\hat{F}_t = \text{Conv}_{1 \times 1}(f_x \odot \sigma(\text{DWConv}_{3 \times 3}(f_a))) \quad (12)$$

where $\sigma(\cdot)$ represents GELU activation, and \odot denotes element-wise product.

C. Convolutional Residual Enhancement Block

Since image resolution is typically increased progressively during up-sampling, previous works [4], [6]–[8] often reduce the number of channels after each stage to maintain a compact network size and acceptable computational cost. However, this approach can lead to a reduction in the number of parameters in later stages, which may hinder the model’s ability to recover fine image details. To address this issue, we integrate convolutional residual enhancement block (CREB) after the final WFUB, which better balances the parameter distribution and enhances the capture of high-level features. The incorporation of residual learning enables the network to focus on reconstructing crucial image details, thereby improving both the model’s capacity and the accuracy of detail restoration.

D. Loss Function

To improve frame detail and structural accuracy, we use a hybrid loss function combining L1 loss and Multi-Scale Structural Similarity Index Measure (MS-SSIM). And to further retention of high-frequency details, we employ frequency constraints to regularize network training, the loss function as:

$$L_{spa} = \alpha \|\hat{I}_t - I_t\|_1 + (1 - \alpha)(1 - \text{MS-SSIM}(\hat{I}_t, I_t)), \quad (13)$$

$$L_{fft} = \|\mathcal{F}(\hat{I}_t) - \mathcal{F}(I_t)\|_1, \quad (14)$$

$$L_{total} = L_{spa} + \mu L_{fft}. \quad (15)$$

Here, \hat{I}_t and I_t represent the reconstructed and original frames, respectively. The symbol $\|\cdot\|_1$ denotes the L_1 -norm, and \mathcal{F} represents the Fast Fourier Transform (FFT). Additionally, α and μ are weight parameters, empirically set to 0.7 and 70, respectively.

III. EXPERIMENTAL RESULTS AND DISCUSSION

A. DataSets and Implementations

We evaluated our approach using the Bunny [20], UVG [21], and DAVIS [22] datasets. The UVG dataset consists of seven video sequences, each with 300 or 600 frames at a resolution of 1080×1920 . For the DAVIS dataset, we used the validation set, which includes 20 videos, each with a resolution of 1080×1920 . The decoder stride was set to [5, 2, 2, 2, 2] for the Bunny dataset and [5, 2, 2, 2, 2] for UVG and DAVIS. For evaluation, we used Peak Signal-to-Noise Ratio (PSNR) and Multi-Scale Structural Similarity Index Measure (MS-SSIM) to assess distortion and measured the video compression bit rate in bits per pixel (bpp). Our method was benchmarked against four NeRV-based approaches with publicly available codes: NeRV [4], E-NeRV [6], HNeRV [7], and boosted HNeRV (Boost) [8]. To ensure a fair comparison, we adjusted the number of channels in each method to maintain consistent overall capacity across the experimental models. Training was performed using the Adan optimizer [23] with a cosine learning rate decay, starting from an initial learning rate of 3×10^{-3} . The batch size was set to 1. All experiments were implemented in PyTorch and executed on a single NVIDIA GTX 4090 GPU, with a model size of 3M and 300 training epochs unless otherwise specified.

TABLE I
PSNR WITH VARYING MODEL SIZE AND EPOCHS ON BUNNY.

Method	Model Size			Epoch		
	0.75M	1.5M	3M	300	600	1200
NeRV	28.46	30.87	33.21	33.21	34.47	35.07
E-NeRV	30.95	32.09	36.72	36.72	38.20	39.48
HNeRV	32.18	35.19	37.43	37.43	39.36	40.02
Boost	35.53	38.95	41.50	41.50	42.03	42.34
Ours	35.82	39.10	41.82	41.82	42.40	42.73

B. Results

1) *Video regression*: We evaluated the video regression performance of our method against other approaches on the Bunny and UVG datasets. As shown in Table I, our method consistently achieved superior video reconstruction quality on the Bunny dataset across various model sizes. Additionally, performance analysis over training iterations reveals that our method converges faster and sustains higher performance throughout training. For the UVG dataset, the results presented in Table II demonstrate that our method attained the highest average performance across all video. Notably, it improved the average PSNR by 0.64 dB at a resolution of 960×1920 and by 0.22 dB at 480×960 compared to the next best method. Fig. 2 (first row) illustrates our method’s ability to preserve fine video details, such as reconstructing text and facial features more effectively than competing approaches. These results underscore the significant impact of the frequency enhancement strategy in improving frame reconstruction quality, highlighting the superiority and robustness of our approach.

2) *Video Compression*: We employed the consistent entropy minimization method [8] for model compression training. Each model was fine-tuned for 100 iterations using an initial learning rate of 5×10^{-4} with a cosine decay schedule. Our approach was benchmarked against two traditional codecs, H.264 [24] and H.265 [25], using FFmpeg with the “very slow” presets. Rate-distortion (R-D) curves, evaluated using PSNR and MS-SSIM metrics on the average of the UVG dataset, are shown in Fig. 3. The results indicate that, at equivalent bit rates, our method consistently surpasses both



Fig. 2. The visualization comparison results are arranged in a top-to-bottom format, highlighting video reconstruction, interpolation, central inpainting (Mask-C), and dispersed inpainting (Mask-S) tasks on the DAVIS validation and UVG datasets. The first column shows the ground truth, followed by the baseline results from NeRV, HNeRV, and our method. The red numbers represent the corresponding PSNR values.

TABLE II
VIDEO REGRESSION PERFORMANCE IN TERMS OF PSNR AND MS-SSIM ON DIFFERENT RESOLUTION UVG DATASET

Resolution	Method	Beauty	Honey.	Bosph.	Yacht.	Ready.	Jockey	Shake.	Avg.
1920×960	NeRV	33.25/0.8886	37.26/0.9794	33.22/0.9305	28.03/0.8726	24.84/0.8310	31.74/0.8874	33.08/0.9325	31.63/0.9031
	E-NeRV	33.53/0.8958	39.04/0.9845	33.81/0.9442	27.74/0.8951	24.09/0.8515	29.35/0.8805	34.54/0.9467	31.73/0.9140
	Hnerv	33.58/0.8941	38.96/0.9844	34.73/0.9451	29.26/0.8907	25.74/0.8420	32.04/0.8802	34.57/0.9450	32.69/0.9116
	Boost	33.93/0.9006	39.62/0.9854	36.00/0.9652	29.69/0.9079	28.33/0.9173	34.51/0.9326	35.89/0.9581	34.00/0.9382
	Ours	34.11/0.9032	39.69/0.9854	37.09/0.9729	30.58/0.9230	29.68/0.9367	35.36/0.9438	35.97/0.9589	34.64/0.9463
960×480	NeRV	32.38/0.9346	36.64/0.9912	32.95/0.9577	28.07/0.9183	24.55/0.8884	31.33/0.9154	32.74/0.9603	31.24/0.9380
	E-NeRV	32.59/0.9399	38.47/0.9936	33.72/0.9705	27.86/0.9393	24.05/0.9069	28.98/0.9084	34.06/0.9715	31.39/0.9472
	Hnerv	32.81/0.9341	38.52/0.9936	34.58/0.9703	29.24/0.9354	25.73/0.9112	32.04/0.9151	34.34/0.9698	32.47/0.9470
	Boost	33.06/0.9437	38.96/0.9942	36.41/0.9843	30.10/0.9512	28.80/0.9603	34.29/0.9570	35.25/0.9768	33.84/0.9668
	Ours	33.48/0.9462	39.17/0.9958	36.64/0.9858	30.40/0.9557	29.28/0.9693	34.83/0.9647	35.81/0.9793	34.23/0.9710

traditional codecs and other NeRV-based approaches, achieving superior compression efficiency.

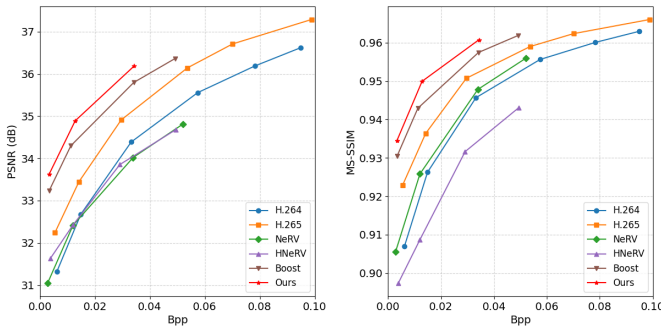


Fig. 3. The rate-distortion curve on UVG in terms of PSNR and MS-SSIM.

3) *video Interpolation*: We evaluated the video interpolation performance of our method on the UVG dataset. Even frames were used for training, while odd frames served as the test set. Table III presents the quantitative results, showing that our method achieved the highest PSNR scores across most video sequences. The qualitative results, illustrated in Fig. 2 (second row), demonstrates that only our method successfully reconstructed the gate numbers on the horse racing starting gates with high fidelity. These results indicate that our method demonstrated superior performance compared to competing approaches in terms of overall interpolation quality.

TABLE III
VIDEO INTERPOLATION RESULTS ON UVG DATASET IN PSNR.

Method	Beauty	Bosph.	Honey.	Jockey	Ready.	Yacht.	Shake.
NeRV	31.26	32.21	36.84	22.24	20.05	26.09	32.09
E-NeRV	31.25	33.36	38.62	22.35	20.08	26.74	32.82
Hnerv	31.42	34.00	39.07	23.02	20.71	26.74	32.58
Boost	31.59	35.92	39.32	22.95	21.34	27.98	32.65
Ours	31.67	36.48	39.22	23.56	22.43	27.87	32.92

4) *Video Inpainting*: We evaluated the performance of FANeRV on video inpainting tasks using the DAVIS validation dataset. We conducted both disperse (Mask-S) and central masking (Mask-C) experiments. In the disperse masking setup, five 50×50 regions were masked in each video frame during training. For the central masking experiment, a region covering

TABLE IV
VIDEO INPAINTING RESULTS ON DAVIS DATASET IN PSNR.

Method	Black.	Break.	Camel	Car-r.	Car-s.	Goat	Kite.	Libby	Para.
Mask-C									
NeRV	24.11	20.16	21.21	21.24	23.07	22.03	23.92	25.71	25.95
E-NeRV	26.38	22.15	22.62	22.73	23.21	23.43	26.71	26.91	26.65
HNeRV	26.45	20.23	17.74	21.71	21.05	23.06	24.73	23.39	26.00
Boost	29.18	20.24	19.81	22.36	23.65	25.10	27.49	26.96	28.07
Ours	29.52	20.61	21.30	22.41	23.69	25.22	27.71	27.73	28.68
Mask-S									
NeRV	27.06	25.48	23.70	23.92	26.58	24.04	29.34	29.81	29.03
E-NeRV	29.53	26.97	25.70	26.32	30.63	25.34	32.87	31.39	30.62
HNeRV	30.20	26.34	26.13	28.64	31.01	26.91	33.49	28.66	30.99
Boost	34.10	33.10	31.08	31.90	35.85	30.59	37.08	37.35	33.64
Ours	35.30	32.78	31.87	32.26	36.58	31.33	37.26	38.27	34.54

one-quarter of the video’s width and height was masked. The training goal was to reconstruct the complete video frame. Table IV and Fig.2 present the quantitative and qualitative results, showing that our method’s robust structural design significantly improved the recovery of masked regions compared to previous methods.

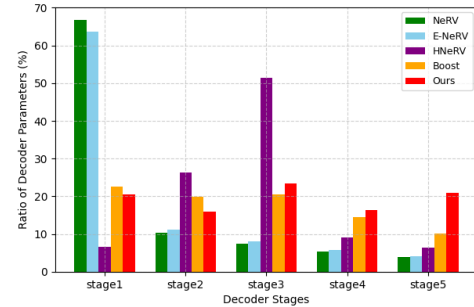


Fig. 4. Parameter distribution across decoder blocks in various models.

5) *Ablation Study*: Tab.V demonstrates the effectiveness of each component in the proposed FANeRV. Multiple variants of the original model were generated and trained on the Bunny dataset to ensure fair comparisons. Initially, individual modules (WFUB, FSFB, TGFN, and CREB) were disabled to evaluate their contributions by comparing their performance to the baseline FANeRV. The results in Table V show significant drops in PSNR values, highlighting the critical role of each module. Additionally, we visualized the decoder parameter

TABLE V
ABLATION STUDY OF FANeRV ON BUNNY DATASET, WITH RESULTS PRESENTED IN PSNR AND MS-SSIM.

Metric	Ours	w/o WFUB	w/o FSFB	w/o TGFN	w/o CREB	w/ Large-kernels conv	w/ Self-attention	w/ ConvTranspose	w/ Bilinear
PSNR	41.82	41.32	41.44	41.58	41.51	41.72	41.65	41.57	40.89
SSIM	0.9942	0.9933	0.9936	0.9937	0.9939	0.9940	0.9935	0.9938	0.9929

distribution at different stages in Fig. 4, showing that our block achieves a more uniform parameter distribution and that the increased parameters in later stages aid in finer detail recovery. Furthermore, we replaced the multi-resolution deep feature modulation branch with large convolutional kernels and channel-wise self-attention mechanisms. This modification led to reduced PSNR values, demonstrating that our approach effectively captures long-range dependencies while maintaining computational efficiency. To further evaluate the multi-resolution fusion strategy, we replaced it with transposed convolution and bilinear upsampling methods. The results confirm that our fusion strategy delivers superior performance. These ablation studies underline the importance of each module in FANeRV and validate the robustness of its overall design.

IV. CONCLUSION

In this paper, we introduce Frequency Separation and Augmentation based Neural Representation for video, which explicitly separates high and low-frequency information and develops distinct recovery methods tailored to their specific characteristics. Extensive experimental results show that FANeRV outperforms several typical methods in reconstruction performance while maintaining the same model capacity.

REFERENCES

- [1] Ben Mildenhall, Pratul P Srinivasan, Matthew Tancik, Jonathan T Barron, Ravi Ramamoorthi, and Ren Ng, “Nerf: Representing scenes as neural radiance fields for view synthesis,” *Communications of the ACM*, vol. 65, no. 1, pp. 99–106, 2021.
- [2] Vincent Sitzmann, Julien Martel, Alexander Bergman, David Lindell, and Gordon Wetzstein, “Implicit neural representations with periodic activation functions,” *Advances in neural information processing systems*, vol. 33, pp. 7462–7473, 2020.
- [3] Vincent Sitzmann, Michael Zollhöfer, and Gordon Wetzstein, “Scene representation networks: Continuous 3d-structure-aware neural scene representations,” *Advances in Neural Information Processing Systems*, vol. 32, 2019.
- [4] Hao Chen, Bo He, Hanyu Wang, Yixuan Ren, Ser Nam Lim, and Abhinav Shrivastava, “Nerv: Neural representations for videos,” *Advances in Neural Information Processing Systems*, vol. 34, pp. 21557–21568, 2021.
- [5] Emilien Dupont, Adam Goliński, Milad Alizadeh, Yee Whye Teh, and Arnaud Doucet, “Coin: Compression with implicit neural representations,” *arXiv preprint arXiv:2103.03123*, 2021.
- [6] Zizhang Li, Mengmeng Wang, Huaijin Pi, Kechun Xu, Jianbiao Mei, and Yong Liu, “E-nerv: Expedite neural video representation with disentangled spatial-temporal context,” in *European Conference on Computer Vision*. Springer, 2022, pp. 267–284.
- [7] Hao Chen, Matthew Gwilliam, Ser-Nam Lim, and Abhinav Shrivastava, “Hnerv: A hybrid neural representation for videos,” in *Proceedings of the IEEE/CVF Conference on Computer Vision and Pattern Recognition*, 2023, pp. 10270–10279.
- [8] Xinjie Zhang, Ren Yang, Dailan He, Xingtong Ge, Tongda Xu, Yan Wang, Hongwei Qin, and Jun Zhang, “Boosting neural representations for videos with a conditional decoder,” in *Proceedings of the IEEE/CVF Conference on Computer Vision and Pattern Recognition (CVPR)*, June 2024, pp. 2556–2566.
- [9] Nasim Rahaman, Aristide Baratin, Devansh Arpit, Felix Draxler, Min Lin, Fred Hamprecht, Yoshua Bengio, and Aaron Courville, “On the spectral bias of neural networks,” in *International Conference on Machine Learning*. PMLR, 2019, pp. 5301–5310.
- [10] Yunjie Xu, Xiang Feng, Feiwei Qin, Ruiquan Ge, Yong Peng, and Changmiao Wang, “Vq-nerv: A vector quantized neural representation for videos,” *arXiv preprint arXiv:2403.12401*, 2024, unpublished.
- [11] Chang Wu, Guancheng Quan, Gang He, Xin-Quan Lai, Yunsong Li, Wenxin Yu, Xianmeng Lin, and Cheng Yang, “Qs-nerv: Real-time quality-scalable decoding with neural representation for videos,” in *Proceedings of the 32nd ACM International Conference on Multimedia*, 2024, pp. 2584–2592.
- [12] Jina Kim, Jihoo Lee, and Je-Won Kang, “Snerv: Spectra-preserving neural representation for video,” in *European Conference on Computer Vision*. Springer, 2025, pp. 332–348.
- [13] Ahmed Ghorbel, Wassim Hamidouche, and Luce Morin, “Nerv++: An enhanced implicit neural video representation,” *arXiv preprint arXiv:2402.18305*, 2024, unpublished.
- [14] Zhuang Liu, Hanzi Mao, Chao-Yuan Wu, Christoph Feichtenhofer, Trevor Darrell, and Saining Xie, “A convnet for the 2020s,” in *Proceedings of the IEEE/CVF conference on computer vision and pattern recognition*, 2022, pp. 11976–11986.
- [15] Kangzhen Yang, Tao Hu, Kexin Dai, Gengeng Chen, Yu Cao, Wei Dong, Peng Wu, Yanning Zhang, and Qingsen Yan, “Crnet: A detail-preserving network for unified image restoration and enhancement task,” *arXiv preprint arXiv:2404.14132*, 2024, unpublished.
- [16] Kai Hu, Yu Liu, Fang Xu, Renhe Liu, Han Wang, and Shenghui Song, “Asymmetric neural image compression with high-preserving information,” in *2024 IEEE International Symposium on Circuits and Systems (ISCAS)*. IEEE, 2024, pp. 1–5.
- [17] Zhisheng Lu, Juncheng Li, Hong Liu, Chaoyan Huang, Linlin Zhang, and Tiejong Zeng, “Transformer for single image super-resolution,” in *Proceedings of the IEEE/CVF conference on computer vision and pattern recognition*, 2022, pp. 457–466.
- [18] Ingrid Daubechies, “The wavelet transform, time-frequency localization and signal analysis,” *IEEE transactions on information theory*, vol. 36, no. 5, pp. 961–1005, 1990.
- [19] Dan Hendrycks and Kevin Gimpel, “Gaussian error linear units (gelus),” *arXiv preprint arXiv:1606.08415*, 2016, unpublished.
- [20] Ton Roosendaal, “Big buck bunny,” in *ACM SIGGRAPH ASIA 2008 computer animation festival*, pp. 62–62, 2008.
- [21] Alexandre Mercat, Marko Viitanen, and Jarno Vanne, “Uvg dataset: 50/120fps 4k sequences for video codec analysis and development,” in *Proceedings of the 11th ACM Multimedia Systems Conference*, 2020, pp. 297–302.
- [22] Federico Perazzi, Jordi Pont-Tuset, Brian McWilliams, Luc Van Gool, Markus Gross, and Alexander Sorkine-Hornung, “A benchmark dataset and evaluation methodology for video object segmentation,” in *Proceedings of the IEEE conference on computer vision and pattern recognition*, 2016, pp. 724–732.
- [23] Xingyu Xie, Pan Zhou, Huan Li, Zhouchen Lin, and Shuicheng Yan, “Adan: Adaptive nesterov momentum algorithm for faster optimizing deep models,” *arXiv preprint arXiv:2208.06677*, 2022.
- [24] Thomas Wiegand, Gary J Sullivan, Gisle Bjontegaard, and Ajay Luthra, “Overview of the h. 264/avc video coding standard,” *IEEE Transactions on circuits and systems for video technology*, vol. 13, no. 7, pp. 560–576, 2003.
- [25] Gary J Sullivan, Jens-Rainer Ohm, Woo-Jin Han, and Thomas Wiegand, “Overview of the high efficiency video coding (hevc) standard,” *IEEE Transactions on circuits and systems for video technology*, vol. 22, no. 12, pp. 1649–1668, 2012.